Susceptor Assisted Microwave Annealing Of

Ion Implanted Silicon

by

Rajitha Vemuri

A Thesis Presented in Partial Fulfillment
of the Requirements for the Degree
Master of Science

Approved April 2011 by the
Graduate Supervisory Committee:

Terry L. Alford, Chair
David Theodore
Stephen Krause

ARIZONA STATE UNIVERSITY

May 2011

©2011 Rajitha Neeha Priyanka Vemuri
All Rights Reserved

ABSTRACT

This thesis discusses the use of low temperature microwave anneal as an alternative technique to recrystallize materials damaged or amorphized due to implantation techniques. The work focuses on the annealing of high-*Z* doped Si wafers that are incapable of attaining high temperatures required for recrystallizing the damaged implanted layers by microwave absorption The increasing necessity for quicker and more efficient processing techniques motivates study of the use of a single frequency applicator microwave cavity along with a Fe_2O_3 infused SiC-alumina susceptor/applicator as an alternative post implantation process. Arsenic implanted Si samples of different dopant concentrations and implantation energies were studied pre and post microwave annealing. A set of as-implanted Si samples were also used to assess the effect of inactive dopants against presence of electrically active dopants on the recrystallization mechanisms. The extent of damage repair and Si recrystallization of the damage caused by arsenic and Si implantation of Si is determined by cross-section transmission electron microscopy and Raman spectroscopy. Dopant activation is evaluated for the As implanted Si by sheet resistance measurements. For the same, secondary ion mass spectroscopy analysis is used to compare the extent of diffusion that results from such microwave annealing with that experienced when using conventional rapid thermal annealing (RTA). Results show that compared to susceptor assisted microwave annealing, RTA caused undesired

dopant diffusion. The SiC-alumina susceptor plays a predominant role in supplying heat to the Si substrate, and acts as an assistor that helps a high-*Z* dopant like arsenic to absorb the microwave energy using a microwave loss mechanism which is a combination of ionic and dipole losses. Comparisons of annealing of the samples were done with and without the use of the susceptor, and confirm the role played by the susceptor, since the samples donot recrystallize when the surface heating mechanism provided by the susceptor is not incorporated. Variable frequency microwave annealing was also performed over the as-implanted Si samples for durations and temperatures higher than the single frequency microwave anneal, but only partial recrystallization of the damaged layer was achieved.

DEDICATION

To my parents Lakshmi and Shashi, who have loved and supported me through all my unconventional decisions, my sister Malini who makes me want to be better at things, my grandparents who brought me up and cared for me like parents, and my husband Shantanu who makes everything worth it.

ACKNOWLEDGMENTS

I am greatly indebted to Dr. Terry Alford for giving me a chance to work in his team before knowing my capabilities. I can't thank enough Mandar Gadre, Anil Indluru, and Karthik Sivaramakrishnan for all the inspiration and support that they have provided. I owe a great part of this thesis to Mandar Gadre, who laid down the foundation for the work.

I express my gratitude to Dr. David Theodore and Prof. Stephen Krause for being in my committee, and taking the time and interest for evaluating my thesis work. I thank Barry Wilkens, Tim Karcher, Klaus Franzeb, Christian Poweleit, and Gordon Tam for their assistance in preparing and characterizing materials in the CSSS facilities.

I would like to thank all my friends and well-wishers who have always been a source of support and positive criticism, for being a part of my life.

This work was partially supported by National Science Foundation (L. Hess, Grant No. DMR-0602716) to whom the authors are greatly indebted. Research was sponsored by the Army Research Laboratory (ARL) and was accomplished under Cooperative Agreement No. W911NG-04-2-0005.

TABLE OF CONTENTS

Page

LIST OF TABLES

LIST OF FIGURES

Figure Page

Chapter 1

INTRODUCTION

1.1 Ion Implantation

Semiconductor materials require impurities to be added to them, to increase their conductivity. Impurities added to the materials, such as silicon are called dopants. Ion implantation is the most practical technique used in the industry to introduce dopants into silicon, since it is controllable and reproducible [1]. Various other methods used to introduce dopants, such as solid-source or gas diffusion have been found to be difficult to control and unreliable. An additional limitation to these methods is that they can incorporate dopants only upto the solid solubility level. However, using ion implantation dopants can be introduced at values above solid solubility.

1.1.a Damage

Ion implantation is performed by vaporizing and ionizing a source of the desired dopant. The ionized atoms are filtered using a mass analyzer and act as a highly pure source for ions used for implantation. These ions, then under a strong electric field, are directed through a beam which is focused onto the Si surface. Before the dopants are directed onto the surface, there is an exchange of energy that occurs between atoms and the electrons due to collisions, and also the atoms come to rest under the

Si surface due to loss of energy [2]. The loss of energy of the ions could be due to nuclear stopping and electronic stopping. The elastic scattering between the ions and the nuclei determine nuclear stopping, whereas for the electron stopping since the ions interact with the electrons in the crystal, inelastic scattering should also be taken into consideration. Ionization of the implanted ions and Si atoms in the target, and excitation of valence band and conduction band electrons can be caused due to these events.

The total distance that the dopant ions travel inside the silicon is calculated by using the two stopping methods used above. The depth at which the dopants reside below the target surface is also determined by the angle of implantation and the energy. The implantation dosage which is the number of dopant atoms incorporated into the silicon per unit surface area is determined by the beam current and implant time. The important parameters of ion implantation are the projected range and projected straggle, which are the average depth of penetration of the dopants, and the deviation from the projected depth respectively.

Collision of the dopant atoms with the silicon lattice displaces the silicon atoms, removing the long range order of the lattice. Displaced atoms with sufficient energy can then collide with other atoms causing them to be displaced and creating a damage profile. The mass of the

dopant atoms also impacts the doping profile [3], apart from the dosage and implantation energy, implying heavier atoms create a greater damage profile. If the long range order is destroyed by a great extent, the silicon surface changes from being crystalline to amorphous.

1.1.b. Complications

Silicon (001) wafers have been used in this study for processing. For a (001) Si surface, a zero degree implantation angle against the normal to the sample results in maximum channeling [4]. While ion implanting the surface, a 7 degree shift from the normal is done to ensure that the dopant atoms such as boron, phosphorous or arsenic are not channeling, or the channeling is minimized. Reducing implant energy to reduce the damage profile makes the implantation process complex [5]. It is necessary for the dopants to have lower energies for a shallow implant region, but the energy is required to be high enough so that the dopant atoms penetrate the Si surface. These conditions set a limit to the minimum energy that can be used for implantation. However, if the implant dose is high, low energies are also sufficient to amorphize the surface.

1.2. Thin film and Shallow Depth Transistors

Thin crystalline Si film structures have gained increased importance in semiconductor industry since the advent of thin film transistors (TFTs) in the 1980s. Crucial regions such as drain/source in ultra-shallow transistors require thin crystalline layers that are highly doped [6, 7] in order to provide the necessary conductivity in these regions. However, heavy implantation damages the surface to the extent of amorphization [8]. It is necessary to repair this damage to make the films crystalline, and to electrically activate the dopants for the devices to function as desired. However, any post implant process should not cause extensive dopant diffusion. Different types of post implantation annealing methods were successful earlier in obtaining solid phase epitaxy (SPE) [9, 10], most widely used of which are laser annealing [11], rapid thermal annealing (RTA) [12, 13], and metal induced crystallization (MIC) [14]. A temperature of above 600^{o}C [15] is required to achieve high quality crystalline Si, which took long hours under conventional furnace annealing. Laser annealing, though extensively used earlier, provides uneven heating of the sample [11]. During laser annealing, a laser beam is focused onto the sample, and the photons that comprise the beam provide energy to the lattice. The lattice reorders itself and makes a long range order crystalline material. But this process transfers heat from layer to layer in a conductive manner, and might not provide uniform heating across the depth of the sample.

Furthermore, the high energy beam might create high temperatures at the surface causing the sample to melt, for instance a temperature of over 1100 ^{o}C can melt the silicon sample, and makes it recrystallize off of the lattice of the substrate material into a polycrystalline. The MIC anneal is known to crystallize Si at lower temperatures and shorter duration; but, it is susceptible to contamination of the ultra shallow film leading to failure of the device [16]. Metals such as aluminium and gold are called eutectic forming metals that have been primarily used as added impurities in the amorphous semiconductor layer to provide local heating sites for the surrounding atoms since the metal atoms heat quicker than the remaining structure. Also, some metals like Ni used in MIC are called silicide forming metals, which are used as capping on the amorphous silicon layer forming silicides upon heating. Recrystallization of the amorphous Si is induced by the silicide seed, and the misfit between $NiSi_2$ and Si and the chemical potential difference between the $NiSi_2$/a-Si and $NiSi_2$/c-Si interfaces. But with ultra sensitive channel layers the minimum amounts of the impurities also cause high channel leakage currents undesired for the functioning of the device.

Rapid thermal anneal mechanism provides high temperatures in short time durations that provides heating across the depth of the material and brings about recrystallization and dopant activation necessary to provide conductive layers. This technique has been effective till the 100

nm technology node where the excessive heat supplied to the dopant atoms not only allows it to settle in the substitutional sites of the lattice, but also forces it deeper into the substrate by a few nanometers. But, as we continue to scale and approach the 17 nm node, the dopant diffusion through RTA would produce junctions which are no more shallow and void their effectiveness.

Hence, as the techonology is scaled to smaller dimensions of technology nodes and the feature sizes, the pre and post implantation processing of materials also need attention. The technology of assisted microwave annealing aims at incorporating the physics behind the quick recrystallization that some of the processing techniques offer but without contaminating the sample, or using extremely high or non-uniform heating.

1.3. Microwaves technology

Methods that activate dopants without causing diffusion are the requirement of the industry inorder to meet ITRS predictions. In this thesis work, we have explored the potential use of low temperature microwave annealing (by use of a Fe_2O_3 infused SiC-Al_2O_3 susceptor/ assistor) as a post implantation technique to achieve solid phase epitaxy (SPE) and dopant activation in arsenic implanted Si. Microwaves function based on

the loss mechanisms which depend on the dielectric properties of the samples/objects being heated/annealed.

1.3.a. Microwave Loss Mechanisms

The sample heating when subjected to microwave radiation occurs as a result of ionic conduction and dipole polarization losses [17]. These losses vary with frequency, and hence the heating profile of the sample varies with different frequencies. In ionic materials, ionic conduction losses or vibrational losses are prominent. Different responses can be observed when ionic materials are subjected to an electric field. In presence of an electric field, electrons move freely inside conductors resulting in electric current. In dielectrics materials, electrons do not move freely and instead, reorientation of induced dipoles gives rise to heating.

Ions move between vacant sites and interstitial positions within the lattice network, leading to space charge effects. But at higher frequencies, vibration losses from the vibration of ions become important, and the frequency dependence of the losses decreases, and becomes more temperature dependent [18]. In the presence of an electric field, the electron cloud in the atom can be displaced with respect to the nucleus, leaving negative charges at one side, and the positive charges at the other side of the atom. An electric dipole moment is created as a result of the

displacement of the uncompensated charges. The summation of the dipoles gives the polarization *P* over a unit volume. In a molecular scale, displacement of charged ions with respect to one another gives rise to dipole moments in in the molecule which comprise the atomic and ionic polarizations.

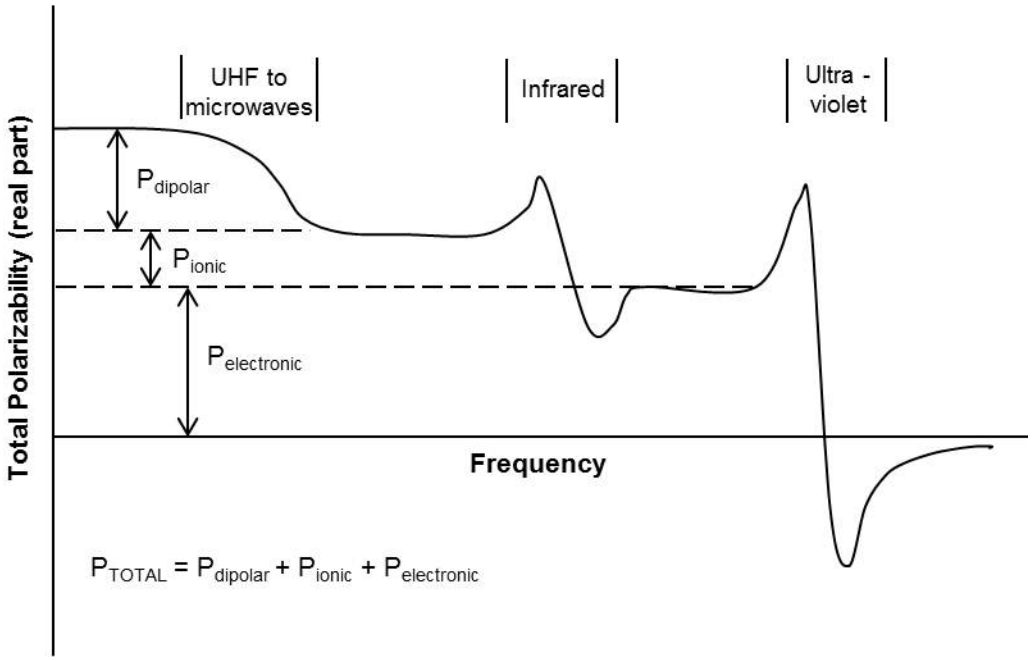

Fig. 1.1 Frequency dependence of different components of polarizability [18]

The ability of a material to absorb electrical potential energy or the microwave field is determined by its complex permittivity. The real part of the permittivity, $\in'$, the depth of penetration of the microwaves into the material can be given, and,the loss factor, $\in''$ [19], indicates the material's

ability to store the energy. *tanδ* is described as the loss tangent that suggests the capability of material to convert the field or energy absorbed into heat.

1.4. High Z Materials

In the past, microwave anneal technology has been used to anneal boron implanted Si with much success.[20] This study is unique compared to other such work done due to the anneal of a higher Z material such as arsenic implanted Si. Due to the higher Z nature of the dopant, greater amount of energy would be required to electrically activate the dopant, by making it lose an electron to the lattice, and also relocate itself substitutionally once the lattice structure has been reformed by recrystallization. To provide energy through heat to facilitate this action, the microwave field generated by a 1300 W, 2.45 GHz magnetron was found to be insufficient. The Si sample by means of having a low dielectric constant is heated by the microwave radiation by volumetric heating, due to larger depth of penetration. With a high depth of penetration, D_P, the sample is incapable of being raised to high temperatures required for recrystallization, 600C being the temperature for Si. The use of a high dielectric assistor material called as a susceptor has been suggested. The susceptor is a cylindrical structure made up of Fe_2O_3 infused SiC surrounding alumina. The structure has high dielectric constant, and when

tested as stand-alone substance being subjected to the microwave radiation exhibits a high temperature heating profile versus time, allowing the surface of the material to be red hot, indicating surface heating by means of low depth of penetration, instead of volumetric heating that provides high depth of penetration. The idea is to supply the heat to the Si sample in a conductive manner so that the sample reaches the temperatures required for recrystallization, and undergoes uniform damage repair due to the uniform absorption of microwaves.

Chapter 2

EXPERIMENTAL PROCEDURE

2.1. Sample Preparation

The base samples are *p*-type boron doped, 100 Ω-cm (100) orientated silicon wafers cleaned using the Radio Corporation of America procedure. Eaton Nova NV10-180 batch process ion implanter was used to implant the cleaned Si wafers. Ion implantation was performed while orienting the wafers at 7^{o} with respect to the normal to the incident beam and with a 45^{o} plane twist, so that ion channeling can be minimized. One set of wafers was implanted at room temperature (RT) using 30 keV As^{+} ions and a dose of 5×10^{14} As^{+} cm^{-2}. Another set of wafers was implanted using 30 keV As^{+} ions and a dose of 1×10^{15} As^{+} cm^{-2} dosage. The last set of samples was implanted with a dose of 180 keV 1×10^{15} As^{+} cm^{-2} ions.

Microwave annealing of different dosage arsenic implanted Si samples was done in a single-frequency (2.45 GHz), 2.8×10^{4} cm^{3} cavity applicator microwave system equipped with a 1300 Watt magnetron source. The anneal times ranged between 40-100 seconds for each sample type. A Raytek Compact MID series pyrometer with a spectral response of 8–14 µm was used to monitor the near surface temperature. The emissivity for the samples was adjusted by careful calibration of the

temperature read by the pyrometer against the temperature monitored by a thermocouple.

The Fig. 2.1 shows the microwave setup involving the pyrometer for in-situ temperature measurements of the sample in the cavity. The arsenic implanted Si cannot raise to a temperature needed for recrystallization of Si, hence a susceptor is used. The susceptor being a cylindrical structure needed to be carved for a 1.5 cm × 1.5 cm groove in the center to mount the sample in order to provide uniform surface heating for the sample from underneath.

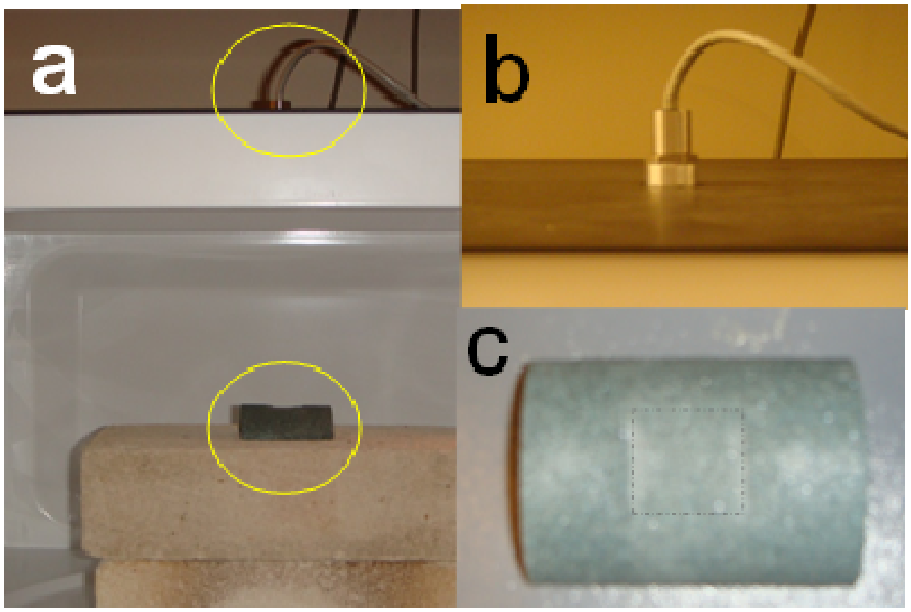

Fig. 2.1 a) The microwave pyrometer-susceptor setup; b) pyrometer to measure in-situ temperature; c) SiC-Al susceptor with a 1.5 cm × 1.5 cm groove to mount the sample to provide uniform heating.

2.2. Material Characterization

With the use of a susceptor to provide additional heating mechanism, the surface temperatures of the arsenic implanted Si ranged between 620-680 ^{o}C. The as-implanted As^{+} and the microwave annealed samples were characterized using several methods to test for dopant activation and film recrystallization. In addition to characterizing pre and post anneal samples for the aforementioned criterion, the microwave annealed samples were compared against 30 second rapid thermal annealed (RTA) samples, annealed at 900℃ for the extent of dopant diffusion. Microwave losses coupled with hybrid volumetric and surface heating of the sample through microwave power absorption and susceptor heating are the mechanisms behind recrystallization of the arsenic implanted Si.

2.2.a Raman Spectroscopy

A Raman line scan was performed to determine the structure of the As^{+} implanted Si pre and post microwave annealing. Raman spectroscopy is one of the most common vibrational spectroscopies to assess the molecular motion. An argon laser with an excitation wavelength of 532 nm is focused onto the samples mounted underneath the optical microscope, through an Olympus 100×0.8 NA objective. The spectra from the sample

are reflected into a Sopra 2000 2m double spectrometer by a 50% beam-splitter. A 532 nm notch filter blocks any scattered light from the laser. The spectrum is dispersed and collected into a Princeton CCD Camera with an energy dispersion of 60pixels/cm. The Raman spectra collected from the CCD is calibrated as a function of intensity that depends on the time of exposure, against the relative wavenumber [21]. High energy beam samples damage the sample surface, but in the Raman spectroscopy, care is taken to avoid usage of high energy beams. The maximum power of a beam used in Raman spectroscopy is 100 mW. In our setup, a 4 mW power beam was used, which goes through a series of beam splitters, at the end of which the beam power hitting the sample is as low as 1 mW which doesn't alter the characteristics of the sample. The setup of the Raman spectroscopy is as seen in Fig. 2.2 below.

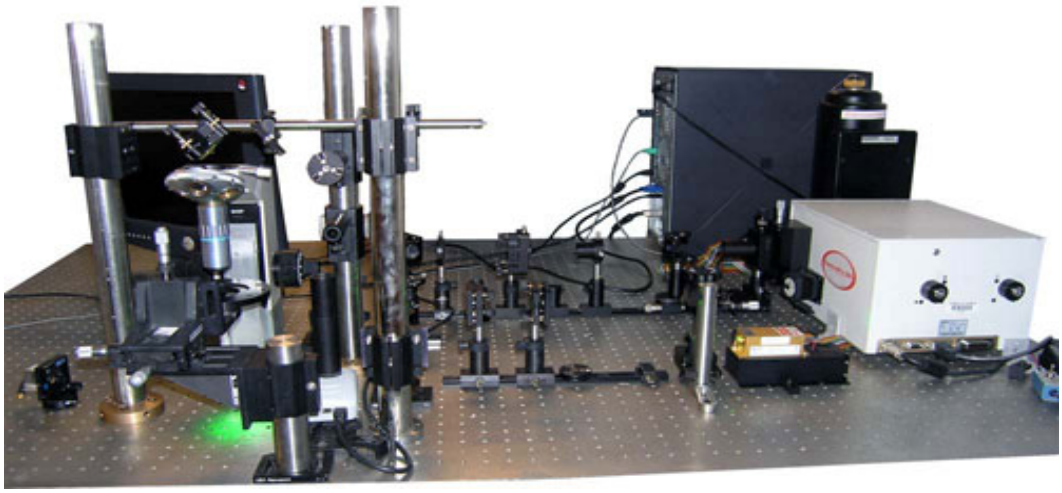

Fig. 2.2 Raman Spectrometer used for characterizing the samples to observe the crystalline structure (Courtesy: Center for Solid State Science, *CSSS,* ASU)

2.2.b Rutherford Backscattering Spectrometry

Rutherford backscattering spectrometry (RBS) is a non-destructive characterization technique. It is used to analyze the atomic composition of the sample like diffusion and interaction between the copper and ruthenium thin films and to estimate the sample thickness using very high energy (MeV) beam of low ion mass. It is also used for quantitative depth profiling, areal density measurements, and determination of crystal lattice quality. RBS utilizes Tandetron accelerator to generate a MeV ion beam. After entering the evacuated beam line, the ions are then collimated and focused. There are bending magnets which after mass selection geometrically disperse ions according to their mass. Finally the beam raster-scans over the specimen and back scattered ions are analyzed by a Si barrier detector. The electronic pulses are then amplified and sorted according to the voltage amplitude by a multichannel analyzer to yield the resulting RBS spectrum [22]. RBS was performed using a General Ionex 1.7 MV tandem accelerator with He^{2+} ions at energy of 2.8 or 3.5 MeV as shown in Fig. 2.3.

Ion implantation with concentrations and energies such as of the samples in our study causes implant damage. Ion channeling experiments were conducted to compare the damage in unannealed samples as

opposed to processed samples, and to ascertain if the microwave annealing could repair damage of this extent. Rutherford backscattering spectrometry (RBS) was used to quantify the implant damage, and a 2.0 MeV He^+ analyzing beam for ion channeling. Samples were analyzed in random and [001] channeled orientations. He^+ ions were collected using a solid state detector, positioned 13^o from the incident beam. The software program RUMP was used to simulate layer thicknesses from RBS data.

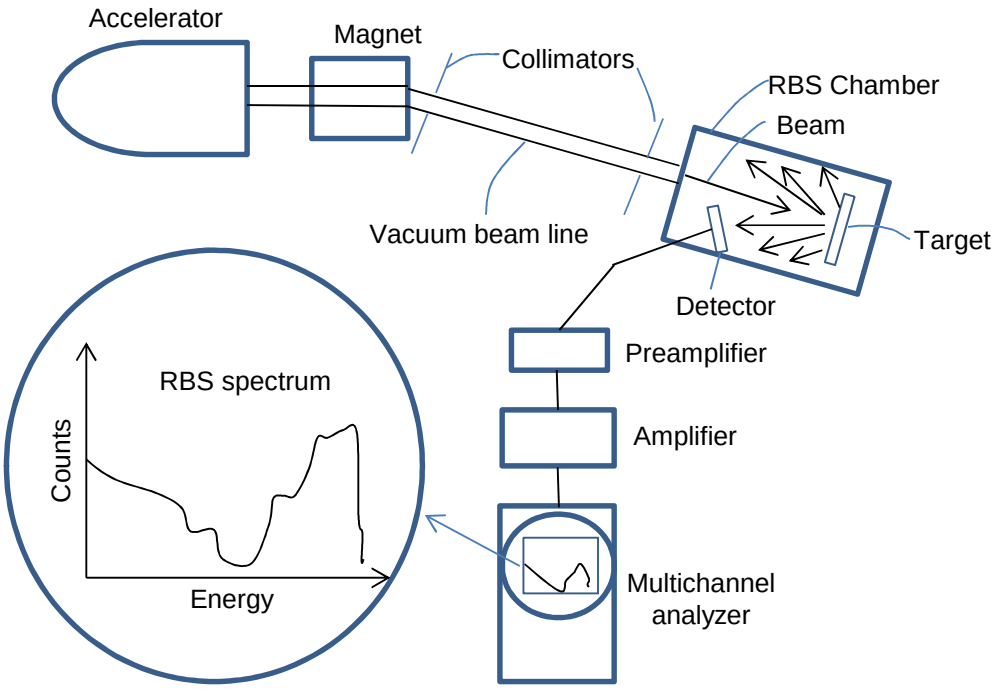

Fig. 2.3 Schematic of a typical Rutherford backscattering Spectrometry instrumentation system.

2.2.c Sheet Resistance Measurement

Sheet resistance of the sample is measured using a typical in line four-point probe configuration as shown in Fig. 2.4. In this method there are totally four probes. The spacing between the probes is 2 nm. Current passes through the outer probes in order to avoid contact resistance and the two inner probes sense the voltage and voltage drop between the two inner probes is measured. Each probe has probe resistance R_p, a probe contact resistance R_{cp} and a spreading resistance R_{sp} associated with it. However, these parasitic resistances can be neglected for the two voltage probes because the voltage is measured with high impedance voltmeter, which draws very little current. Thus the voltage drops across these parasitic resistances are insignificantly small. The voltage reading from the voltmeter is approximately equal to the voltage drop across the material sheet resistance. The sheet resistance is calculated from the measured values of the voltage and the current by dividing the voltage by the current and multiplying this by the correction factor which depends on the probe spacing, film thickness and the probe distance from the edge of the sample. The sheet resistance expressions can be expressed as follows:

$$R_s = (V/ I) \times CF \qquad (1)$$

where CF = Correction factor and V/ I is the reading from the monitor, V is the voltage drop and I is the current driven through the sample.,

The resistivity of the material is calculated by using the following expression:

$$\rho = R_s \times t \qquad (2)$$

where t = thickness of the material. This measurement was of particular interest to verify that the resistance of the alloy films after annealing was comparable to that of the as-deposited sample.

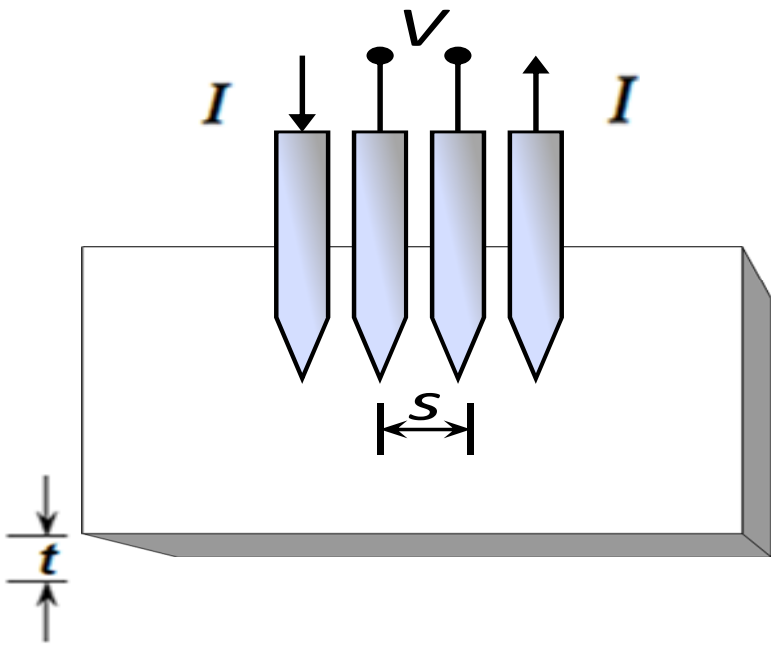

Fig. 2.4: Layout of atypical four-point probe setup. Measurements taken at ASU had a probe spacing of 2 mm. Where S = spacing between the probes, and t = thickness of the sample.

2.2.d Hall Measurements

In order to determine if there was any carrier inversion that occurred after microwave annealing, Hall measurement testing was performed over the samples before and after annealing.using Van der Pauw method. To do so, the samples were mounted onto a printed circuit board by making aluminum deposits for contacts, and using copper wires and silver paste to establish contacts.

The Van der Pauw method is the most common technique used to accurately measure electrical properties of a sample such as the resistivity, doping of the material whether it is p-type or n-type doped, the mobility of the majority carriers, and the sheet carrier densities. To be able to use the Van der Pauw method, the sample thickness needs to be much less than the length and width of the sample, which means, the sample needs to be 2 dimensional. To reduce errors in the measurement, the sample should be made symmetrical, most often a square shaped one. The contacts for the measurement need to be made appropriately too, and the material for contact should be chosen in such a way that an ohmic contact can be made. Silver is used to make contact with between the copper wires and the sample material. But for silicon substrates, silver cannot make an ohmic contact directly, hence aluminum was deposited

using an evaporator system and masks, just at the corners of the sample, and silver can then be used to make the contact with copper wires.

In order to use the Van der Pauw method, the sample thickness must be much less than the width and length of the sample. In order to reduce errors in the calculations, it is preferable that the sample is symmetrical. There must also be no isolated holes within the sample. From the top left corner of the sample, if the contacts are numbered 1 to 4 in a counter-clockwise direction as seen in Fig. 2.5, current is made to flow along one edge of the sample (along the 1-2 side), and voltage is noted on the other edge (along the 3-4 side).

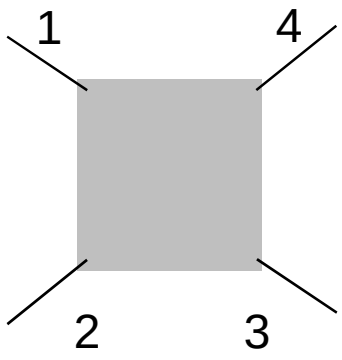

Fig. 2.5: Sample labeling for the contacts made to perform van der Pauw Hall measurements.

The ratio of the voltage V_{34} and I_{12}.gives the resistance in the material

$$R = \frac{V_{34}}{I_{12}} \qquad (3)$$

Hall measurements, as the name suggests, make use of the Hall effect in electrical characterization of the material. When electrons flow through a magnetic field, a force called Lorentz force is exerted on them which depends on the velocity of their motion in the field. The force is maximum when the field is perpendicular to the motion of the electrons, and is given by

$$F_L = q.\upsilon.B \qquad (4)$$

where q = the charge on the particle in coulombs

υ = velocity

B = the strength of the magnetic field (Wb/cm^2)

Applying current on a semiconductor material results in a steady state flow of electrons within the material, with a velocity given by

$$\upsilon = \frac{1}{n_m \mu_m q} \qquad (5)$$

where n = electron density

A = cross-sectional area of the material

$q = 1.6 \times 10^{-19}$ coulombs

The force leads to accumulation of charges along an edge and creates an electric field induced produce accumulation of electrons along an edge, and the hall voltage can be directly extracted from this field, given by

$V_H = \omega \epsilon$ (6)

$= \frac{IB}{nqd}$ d=depth of the material

$= \frac{IB}{n_s q}$

Hence, we can obtain the sheet density n_s from the hall voltage. From previously obtained resistivity measurements, sheet resistance of the material is known from which the mobility of the material is given by

$\mu = \frac{1}{n_s q R_s}$ (7)

Finally the resistivity of the material is given by

$\rho = \frac{1}{n_m \mu_m q}$ (8)

where n_m = doping level of majority carrier

μ_m = mobility of the majority carrier

Seen in Fig. 2.6 below is the setup for the Ecopia HMS 3000 Hall measurement system used in our characterization methods, for which a magnet of 0.98 Tesla was used. To recover the measurements, the magnet was aligned in N-S, S-N directions.

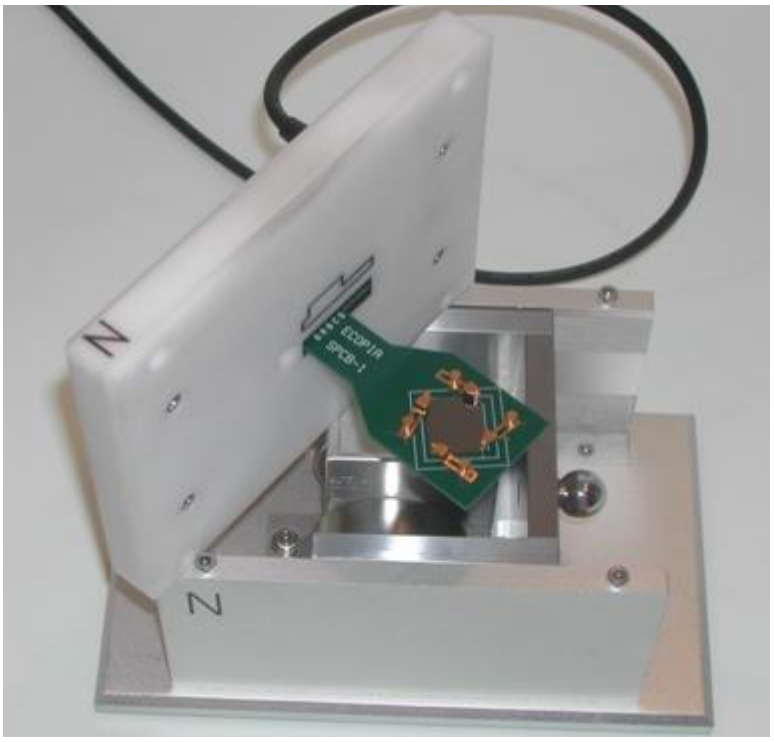

Fig. 2.6 Ecopia HMS-3000 Hall Effect Measurement System used at ASU (Courtesy:*CSSS,* ASU).

2.2.e Cross-section Transmission Electron Microscopy and Focused Ion Beam Milling

Focused Ion Beam milling or FIB milling was performed on the samples, to lift off a nanoscale dimension of the specimen before performing a cross-section transmission electron microscopy (XTEM) on them. Highly energetic ion beams are impinged onto the sample, at an angle of 52°. The beam has sufficient energy to lift off a portion of the sample to create a nanospecimen. The equipment has an electron gun that ensures that the properties of the material are not altered. Highly energy Ga is used to form the focused ion beam. The mechanism can be

programmed to ensure which part of the sample needs to be sputtered out to form a specimen sample. The facility has an inbuilt scanning electron microscope to monitor the lift off process in real time [23]. The schematic of the FEI 835 focused-ion beam tool with a gallium ion-source is seen in the Fig.2.7.

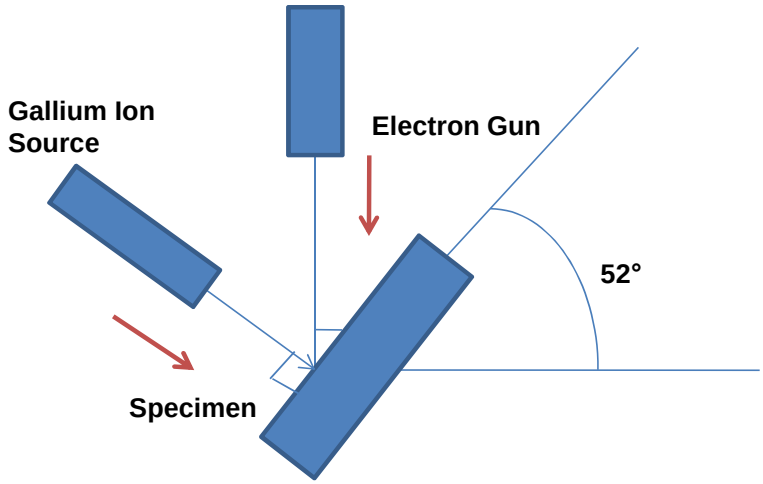

Fig. 2.7 FEI 835 focused-ion beam tool with a Ga ion-source used at ASU

A Philips CM200 FEG TEM operated at a voltage of 200 kV was used to perform cross-sectional transmission electron microscopy on the specimen sample to observe the structure of the material. Seen below is a picture of the TEM available at Arizona State University..

Fig. 2.8 Philips CM200 FEG TEM used at ASU (courtesy *CSSS*)

2.2.f Secondary Ion Mass Spectroscopy

Secondary ion mass spectrometry (SIMS) is a surface analysis technique that can help determine the composition of materials. A primary ion beam is focused onto the sample, and secondary ions ejected are collected. These secondary ions are analyzed are captured by a mass spectrometer to determine the composition of the surface. The yield in terms of time collected by the analyzer is calibrated in terms of concentration of atoms across the depth of the sample. Seen below is a schematic of the direction of focused beam, and placement of the analyzer with respect to the sample surface, to capture the secondary ions.

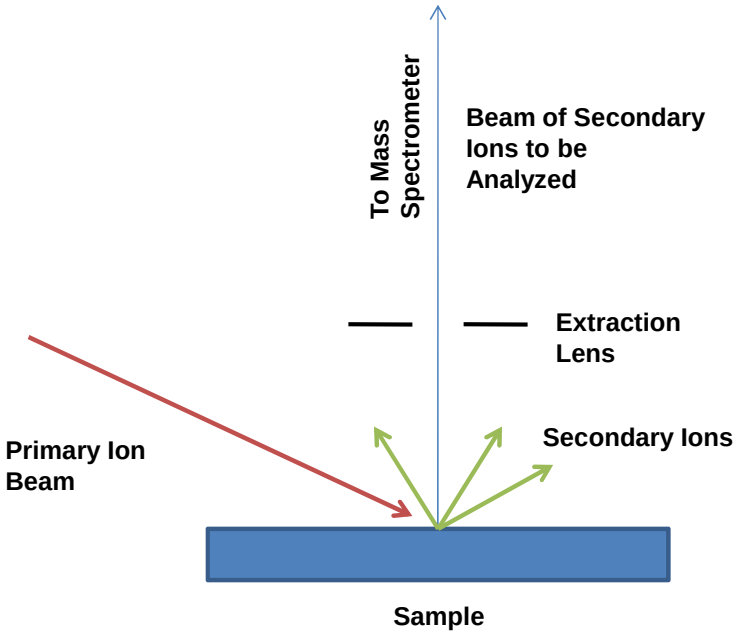

Fig. 2.9 Mechanism of SIMS analyzer

Due to the interaction of the beams with the surface, the upper layers of the sample can get amorphized, some of the atoms of the primary beam can get implanted in the surface of the sample, apart from secondary particles being ejected from the sample. The samples ejected can be neutral as well as positively and negatively ionized. The secondary ions from the sample are extracted by an electric field applied in the region between the sample and an extraction lens. The ions get accelerated in the presence of this field towards a calibrated mass spectrometer. The ions are sorted based on the mass and energy and pass through an ion detector which can be a Faraday cup, where the yield count is obtained.

The rate of the yield can provide information about the composition of the material. The SIMS technique is useful for all elements except noble gases since they don’t ionize easily.

Chapter 3

DOPANT ACTIVATION AND DIFFUSION PROFILE OF ARSENIC IMPLANTED SILICON

3.1. Introduction

To perform quick regrowth or dopant activation by post implantation processing , the semiconductor is intentionally adulterated with additional dopant or metal atoms [24] which act as localized heating spots when annealed, raising to higher temperatures quicker than the semiconductor atoms due to their specific heat properties and Fermi level effects. Regrowth rate becomes greater with temperature, and hence shorter times suffice for recrystallization. Over the years there has been success in the development of processes which achieve this high temperature in shorter hours, and some even in seconds (*e.g.,* RTA), but without adulterating the sample in order to do so. In this study we have used microwave annealing (by using a SiC susceptor/assistor) to achieve a high quality crystalline Si layer in much shorter times, and have compared it against the samples treated using RTA, to verify the reduced extent of end-of-range diffusion. This shallower dopant profile over RTA confirms the potential use of susceptor assisted microwave annealing for dopant activation and solid phase regrowth. The assistor, as the name suggests, is used to supply additional heat to the sample for it to reach the desired temperature range in a shorter time. This study discusses the mechanism

of this heat supply, and the quality of the results produced, if they are better than the results obtained from methods mentioned before.

3.2. Experimental procedure

The base samples are *p*-type boron doped, 100 Ω-cm (100) orientated silicon wafers cleaned using the Radio Corporation of America procedure. Eaton Nova NV10-180 batch process ion implanter was used to implant the cleaned Si wafers. Ion implantation was performed while orienting the wafers at 7^{o} with respect to the normal to the incident beam and with a 45^{o} plane twist, so that ion channeling can be minimized. One set of wafers was implanted at room temperature (RT) using 30 keV As^{+} ions and a dose of 5×10^{14} As^{+} cm^{-2}. Another set of wafers was implanted using 30 keV As^{+} ions and a dose of 1×10^{15} As^{+} cm^{-2} dosage. The last set of samples was implanted with a dose of 180 keV 1×10^{15} As^{+} cm^{-2} ions. Microwave annealing of different dosage arsenic implanted Si samples was done in a single-frequency (2.45 GHz), 2.8×10^{4} cm^{3} cavity applicator microwave system equipped with a 1300 Watt magnetron source. The anneal times ranged between 40-100 seconds for each sample type. A Raytek Compact MID series pyrometer with a spectral response of 8–14 µm was used to monitor the near surface temperature. The emissivity for the samples was adjusted by careful calibration of the temperature read by the pyrometer against the temperature monitored by a thermocouple.

For the arsenic implanted samples, the surface temperatures ranged 620-680 ^{o}C

Ion implantation with concentrations and energies such as of the samples in our study causes implant damage. Ion channeling experiments were conducted to compare the damage in unannealed samples as opposed to processed samples, and to ascertain if the microwave annealing could repair damage of this extent. Rutherford backscattering spectrometry (RBS) was used to quantify the implant damage, and a 2.0 MeV He^{+} analyzing beam for ion channeling. Samples were analyzed in random and [001] channeled orientations. He^{+} ions were collected using a solid state detector, positioned 13^{o} from the incident beam. The software program RUMP was used to simulate layer thicknesses from RBS data.

To test for any electrical dopant activation, the samples were placed face up under an in-line 4 point probe reading out to a 100 mA Keithley 2700 digital multimeter. The sheet resistances (R_{sh}) of the samples were carefully tabulated for every process time. In order to determine if there was any carrier inversion that occurred after microwave annealing, Hall measurement testing was performed over the samples before and after annealing using Van der Pauw method. To do so, the samples were mounted onto a printed circuit board by making aluminum

deposits for contacts, and using copper wires and silver paste to establish contacts.

Secondary ion mass spectroscopy (SIMS) was performed to capture the secondary As^+ ions from the sample across its depth. The results observed as a function of the yield with time were calibrated to give a measure of the density of As^+ across the depth of the sample. The plot of As^+ density as a function of Si depth gives a measure of the extent of diffusion of the dopant for the microwave annealed samples and for RTA annealed samples.

3.3. Results

The anneal time in the study is defined as the duration between when the microwave is switched on and when the microwave is turned off. The temperature profile of the samples suggests that stand alone microwave heating is not sufficient for the samples to reach the required temperatures of around 600 ^oC as mentioned earlier, since *a*-Si cannot absorb microwave energy at low temperatures [16], and supports our incentive of using an additional heating material in the setup to enable the samples to absorb the microwave radiation. Inspection of Fig. 3.1 reveals how microwave radiation assisted by the alumina coated silicon carbide (SiC-alumina) susceptor [16,25], allows for rapid heating and confirms

that microwave annealing without a susceptor does not help the sample obtain a high temperature.

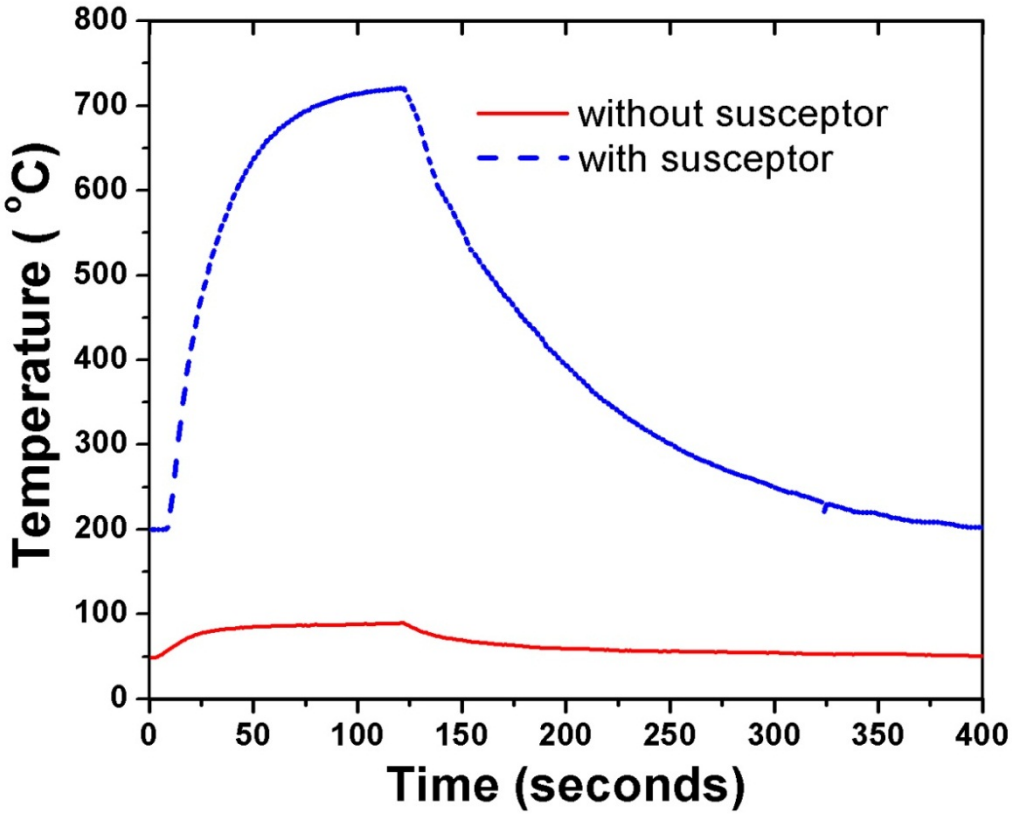

Fig. 3.1 Temperature vs Time profile of As implanted Si with and without susceptor

The spectra *random* and *as-implanted* in Fig. 3.2 present RBS results obtained from the as-implanted samples in a random orientation and a [001] channeling orientation, respectively. The energetic arsenic ions create a thin damaged Si layer and amorphize the crystalline Si. Both the plots show the lattice damage due to ion implantation, and also a magnified (× 30) As peak around channel number 280 [25], that confirms

arsenic is located off the lattice sites instead of at the substitutional sites [20]. A comparison of the normalized yield of aligned channeling spectrum against the normalized yield of random spectra gives the order of lattice damage. The factor is denoted by χ_{min} [26]. Channeling spectrum *annealed* presents ion channeling results of the samples in a [001] channeling orientation after 40 sec microwave annealing. The χ_{min} for *annealed* is 0.11 implying that the lattice damage was repaired to a great extent. The ion channeling yield of a 70 sec annealed sample (not shown), also has a χ_{min} of around 0.11 confirming that the improvement in lattice damage repair is insignificant over a 40 sec microwave anneal. The results signify that the dopant atoms are now essentially located in substitutional sites instead of off-lattice sites, as in the *as-implanted* channeled spectrum in Fig. 3.2. This repair of lattice damage, and dopant relocation, are key factors that lead to dopant activation and reduced sheet resistance of the arsenic implanted Silicon samples. The spectra of 180 keV arsenic implanted samples, confirms deeper lattice damage, and thicker damaged surface layer. However great the damage, a 40 second anneal would still suffice to repair the lattice implant damage, and distribute the dopant atoms to substitutional sites in the lattice.

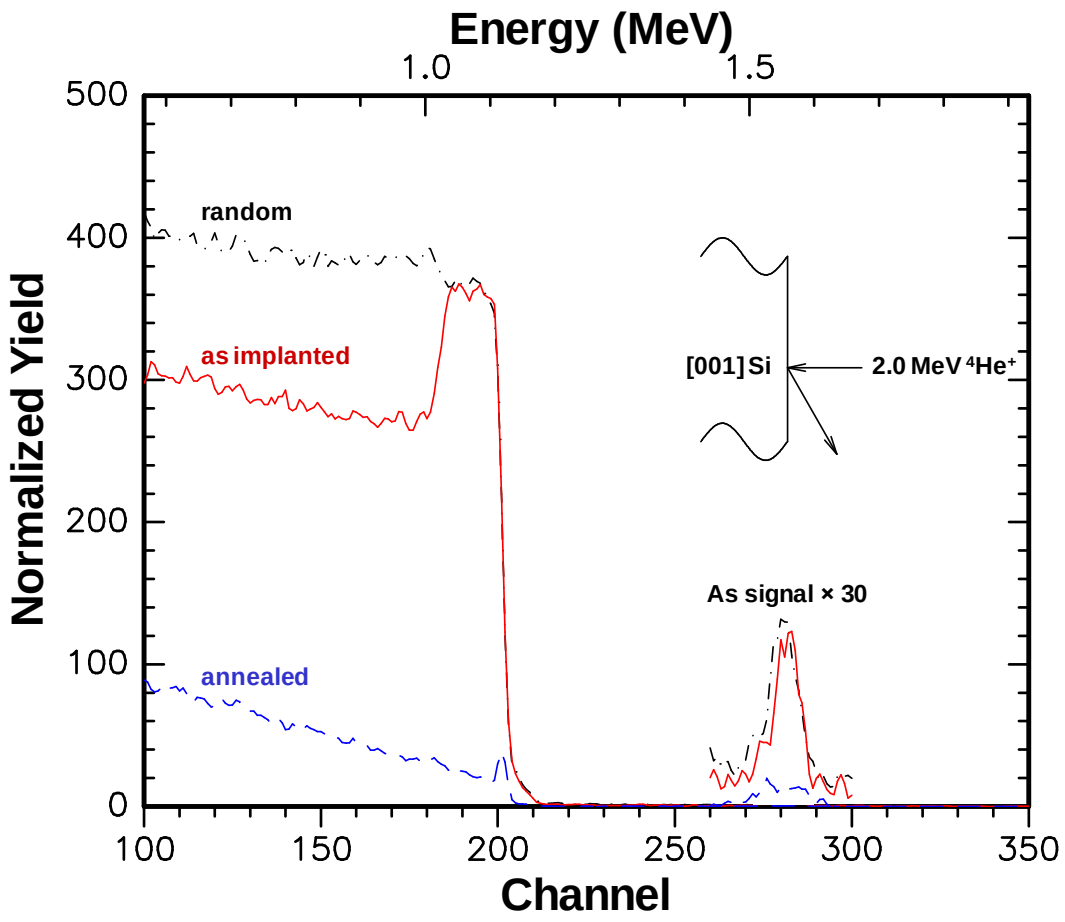

Fig. 3.2. Ion channeling results of As^+ implanted Si: Dotted ***random*** represents ion channeling of 180 keV $1x10^{15}$ as-implanted As^+ sample in random orientation. Solid line ***as implanted*** represents ion channeling of as implanted As^+ in channeling orientation**.** Dotted ***annealed*** represents ion channeling of 180 keV $1x10^{15}$ cm^{-2} arsenic implanted Si annealed for 40s, in channeling orientation. The As signal represented in the analysis has been enhanced 30 times for ***random***, ***as implanted***, and ***annealed*** spectra, and follows the same legend.

Analysis of sheet resistance values of annealed samples against readings from the unannealed samples shows that almost complete dopant activation was achieved within a processing time of 40 sec, beyond which there is no significant improvement, as seen in Table 1.

Implant energy (keV)	Implant dose (1×10^{15} cm^{-2})	Sheet Resistance (Ohm/sq) for different microwave anneal times			
		as-implanted	40 seconds	70 seconds	100 seconds
30	× 0.5	overflow	221	198	188
30	× 1	overflow	140	134	133
180	× 1	overflow	93	86	81

Table 1 Sheet Resistance measurements over different anneal times

This applies to all three samples of different dosages and energies that were included in the study. As seen in the table, before microwave anneal, the 4 point probe reads *overflow* which implies the samples are non-conductive or that their sheet resistance (R_{sh}) is beyond the order of mega Ohm/sq. The Fig.3.3 below shows the pattern of sudden reduction is R_{sh}, which saturates for greater annealing times.

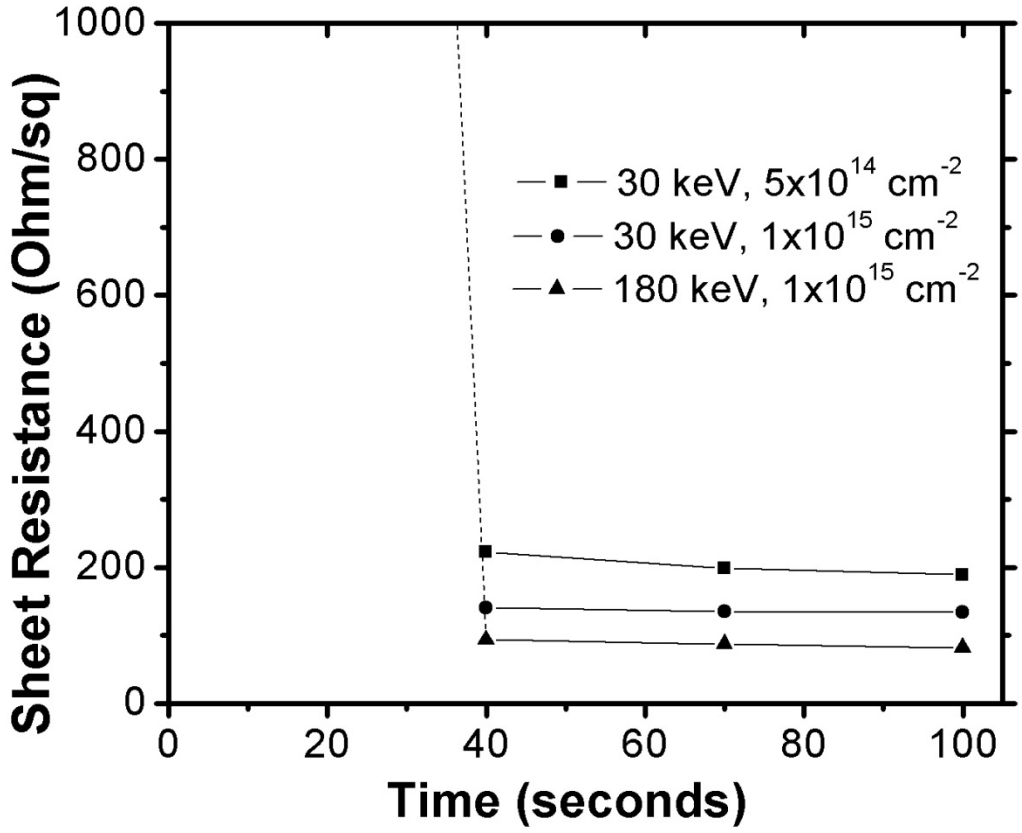

Fig. 3.3. Sheet Resistance measurements of the different dosage and implantation energy As implanted Si at different anneal times.

The Hall measurements show the inversion of carriers from p-type before annealing, which is from the heavily boron doped substrate, to being n-type from the arsenic that was implanted onto Si samples. Due to the heavy doping that causes degenerate sheet concentration values, ion scattering becomes dominant in the surface, reducing the mobilities after annealing, which were otherwise expected to be high. Table 2 summarizes the resistivities, sheet and bulk concentrations, and mobilities

of 30 keV 1×10^{15} As^{+} cm^{-2} and 180 keV 1×10^{15} As^{+} cm^{-2} implanted Si samples. The values of the 30 keV 1×10^{14} As^{+} cm^{-2} fell between those of the sample variety *A* and *B*, but were not discussed in the table.

Sample	Resistivity (Ω cm)	Carrier type	Sheet concentration (# cm^{-2})	Bulk Concentration (# cm^{-3})	Mobility (cm^2 /V-sec)
A and B as-implanted Backside	45	p	6.8×10^{12}	1.7×10^{14}	530
Sample A as-implanted Front	1.3×10^{-3}	p	1.7×10^{14}	3.5×10^{19}	235
Sample A 40 second annealed Front	2.8×10^{-3}	n	8.3×10^{14}	1×10^{20}	53
Sample A 100 second annealed Front	2.7×10^{-3}	n	7.65×10^{14}	1.53×10^{20}	61
Sample B as-implanted Front	13×10^{-3}	p	9.25×10^{13}	3.7×10^{18}	120
Sample B 40 second annealed Front	2.4×10^{-3}	n	9.95×10^{14}	4.0×10^{19}	65
Sample B 100 second annealed Front	2.1×10^{-3}	n	8.2×10^{14}	3.3×10^{19}	89

Table 2 Hall measurement values for **A**: 30 keV 1×10^{15} As^{+} cm^{-2} and **B**: 180 keV 1×10^{15} As^{+} cm^{-2} implanted Si

To assess the impact of susceptor-assisted microwave annealing on dopant diffusion, SIMS analysis was performed on a 900 ^{o}C RTA sample, annealed for 30 seconds, apart from the microwave annealed

samples. As seen in Fig. 3.4, both 40 and 70 seconds microwave annealing on the samples shows minimal dopant diffusion across the depth. RTA on the sample shows greater dopant diffusion possibly as a result of energizing the As^+ to diffuse into the sample.

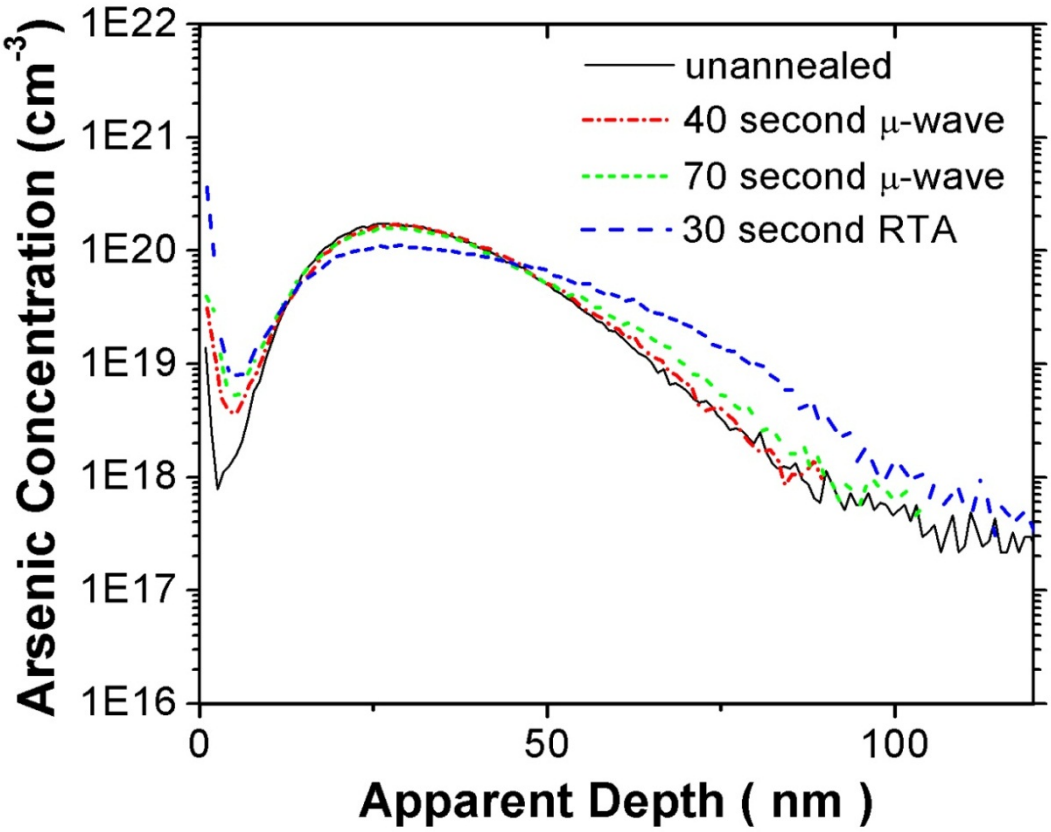

Fig. 3.4 SIMS profile of 30 keV 5×10^{14} As^+ impanted Si annealed under different conditions

3.4. Discussion

The cumulative effect of a few phenomena is responsible for the effectiveness of susceptor-assisted microwave annealing. These can be

categorized into the effect of microwaves, and the effect of the susceptor. Microwaves supply sufficient energy to surmount the high activation energy needed for lattice damage repair and bring about dopant activation, without causing dopant diffusion, all in a short duration. For dopant activation of arsenic to be achieved, the As need to replace Si in the substitutional sites. Our ion channeling results also show that the dopant atoms now occupy substitutional lattice sites suggesting successful dopant activation.

The mechanism underlying the heating of the sample is microwave power loss. Microwave power converts into heat based on the property of the material defined as effective loss factor, which comprises conduction and polarization losses [27]. Depending on the dielectric constant of the sample, the power absorbed and the depth of absorption of the microwave radiation vary [28]. The power thus absorbed is converted into heat based on the specific heat capacity value of the sample. The sample in discussion is arsenic doped Si, As having a C_P of 326 J/Kg-K, and Si having a C_P of 710 J/Kg-K.

Apart from the dielectric constant, the dielectric loss factor of a material is another property that decides its absorption capability. Materials with high dielectric loss factor can absorb microwave radiation better. Thus, considering only the effect of microwave radiation, which

provides volumetric heating, the power absorbed per unit volume is given by equation 1 as

$$\begin{aligned} P_{abs} &= \sigma_{eff} |E|^2 \\ &= \omega \in_0 \in''_{eff} |E|^2 \\ &= \omega \in_0 \in''_r \tan\delta |E|^2 \end{aligned} \qquad (1)$$

where E is the magnitude of the internal electric field, $\in_{eff}$ is the relative effective dielectric factor, $\in_0$ is the permittivity of free space, ω gives the microwave frequency, σ_{eff} is the total effective conductivity, $\in_r$ is the relative dielectric constant, and $tan\delta$ is the energy loss required to store a given quantity of energy [29]. The above relation takes into effect the ionic conduction losses and dipole polarization losses which comprise the overall microwave loss mechanism responsible for absorption of the microwave energy. The ionic conduction losses, also called the ohmic losses arise from the movement of the free electrons available due to the presence of the arsenic dopant atoms, and the dipole polarization losses are as a result of the interaction between the vacancies and interstitials present in the sample. The conversion of the power thus absorbed, into heat based on the material properties follows the relation [30]

$$P = m\, C_P \frac{\Delta T}{\Delta t} \qquad (2)$$

where *m* is the mass. In terms of the dielectric properties of the material, the change in temperature of the sample with time would be [28]

$$\frac{\Delta T}{\Delta t} = \frac{\omega \in_0 \in_r^{"} \tan\delta \,|E|^2}{\rho_{mass} C_P} \qquad (3)$$

For a given material, the factor that can vary at a fixed frequency is $tan\delta$ [31] which is the ratio of the dielectric loss with respect to the dielectric constant. For both a-Si and c-Si this reduces with temperature, as dielectric constant rises with temperature. Hence, in the heating curves of all the samples in this study, we observe that the temperature rises fast initially, and the dielectric constant increases [32] with time, saturating the temperature, as $tan\delta$ reduces.

Microwave radiation provides volumetric heating [29] to the sample, limiting the depth of penetration to D_P which is the depth into the sample, at which the effect of the microwave field reduces by a factor 1/e, or the power absorbed is half as much as it is at the surface of the sample. D_P is given by equation (4)

$$D_P = \frac{3\lambda_0}{8.686\pi \ tan\delta \sqrt{\frac{\acute{\varepsilon}_r}{\varepsilon_0}}} \qquad (4)$$

With the extent of ion implantation damage caused by the energetic arsenic items during doping, the volumetric heating and the depth of penetration of the radiation into the sample is not sufficient to repair the damage by nucleation followed by growth. Furthermore, arsenic being a high *Z* material requires a higher temperature to absorb the microwaves.

The advantages of microwave radiation can be applied to our As implanted Si samples and other high *Z* implanted samples, by including an additional assisting system, that can help the sample obtain a temperature where it can absorb the microwave radiation and further convert the power to heat. The susceptor surely pronounces its effect in the arsenic implanted Si samples, by acting as a source of additional heat, but does not negate the underlying impact of microwave radiation, hence making it an assisted annealing method.

3.5. Conclusion

Through this study, we were able to elucidate in detail how microwave loss mechanisms, high activation energies, and the susceptor, all combine to achieve an electrically active arsenic doped Si thin film layer. Susceptor assisted microwave annealing also proved better than the widely used RTA method, since it led to very low dopant diffusion across the film. With some more improvements, this technique would be a promising replacement in the semiconductor industry.

Chapter 4

RECRYSTALLIZATION OF ARSENIC AND as-IMPLANTED SILICON

4.1. Introduction

Inorder to compare the temperature profiles of a doped sample versus self implanted Si sample without the influence of a susceptor, an as-implanted Si with 75 keV implantation energy, and 2×10^{15} cm^{-2} Si^{+} dosage was also chosen. Figure 4.1 shows a typical plot of temperature as a function of anneal time for a) 180 keV, 1×10^{15} As^{+} cm^{-2} implanted Si sample and b) 75 keV, 2×10^{15} cm^{-2} as implanted Si^{+}, both samples annealed for 2 minutes without a susceptor. The anneal time in the study is defined as the duration between when the microwave is switched on and when the microwave is turned off. The temperature profile of these samples suggests that stand alone microwave heating is not sufficient for them to reach the required temperatures of around 600 ^{o}C as mentioned earlier since *a*-Si cannot absorb microwave energy at low temperatures [16], and necessitates the use of an additional heating material in the setup to enable the samples to absorb the microwave radiation.

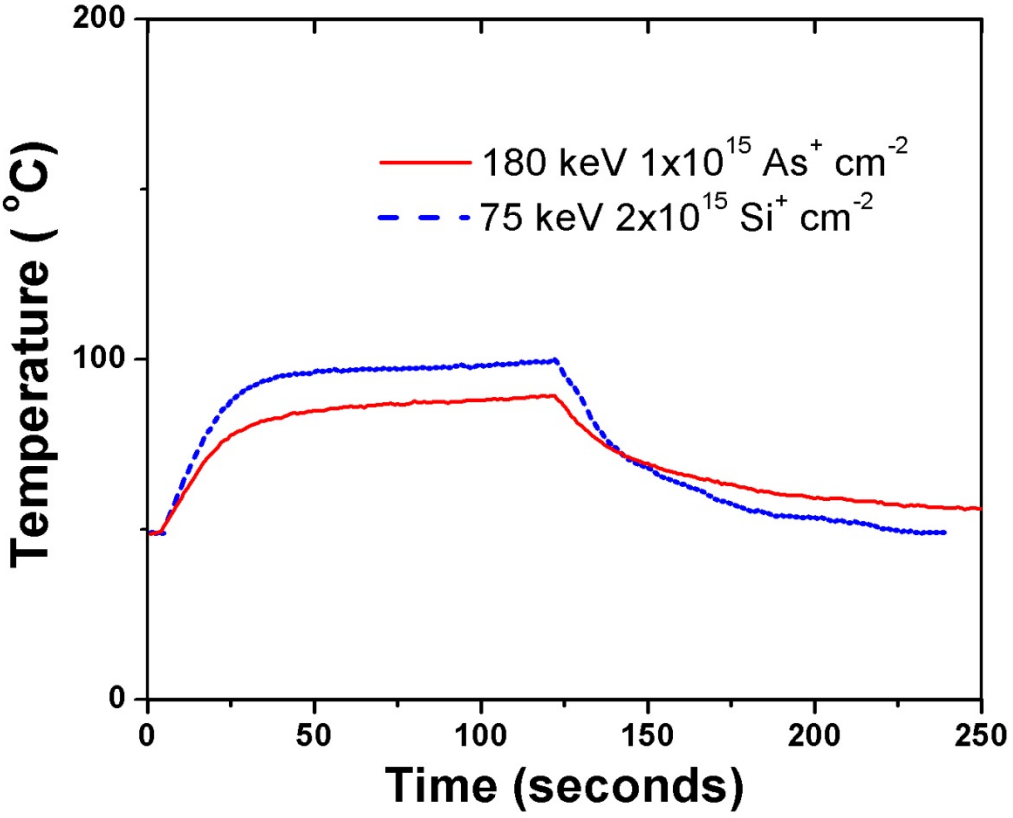

Fig. 4.1 Temperature vs time profile of As implanted Si and as-implanted Si without a susceptor.

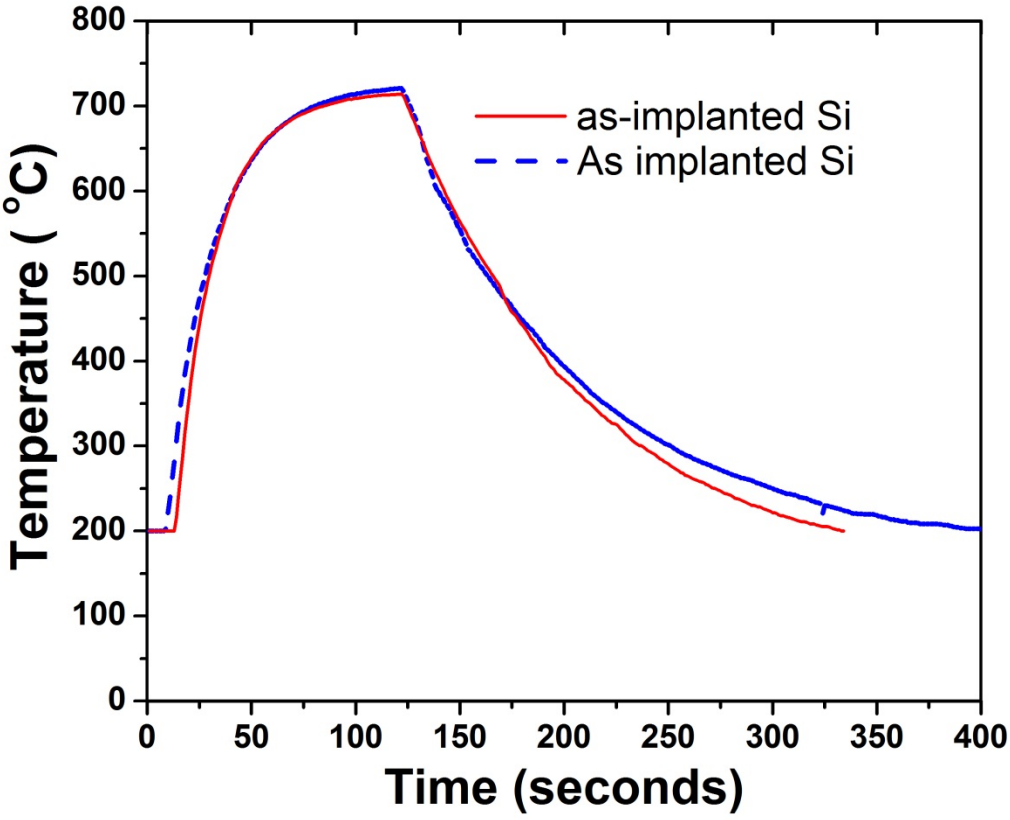

Fig. 4.2 Temperature vs time profile of As implanted Si and as-implanted Si witht a susceptor.

The samples in discussion are arsenic doped Si and as-implanted Si, As having a C_P of 326 J/Kg-K, and Si having a C_P of 710 J/Kg-K. But an atom of Si heats to a higher temperature than an atom of arsenic for the same power absorbed, since Si weighs lesser than arsenic, and the $mC_{P\,(Si)} < mC_{P\,(As)}$. The effect of C_P on heating rate without the assistance of a susceptor can be noticed in Fig.4.1. In order to create the same extent of damage as 180 keV 1×10^{15} cm^{-2} arsenic implanted Si, the as-implanted Si was formed by implanting with 75 keV 2×10^{15} cm^{-2} Si^{+}. The

dosage [33] of Si^+ chosen produced the same depth of the damage layer as did the As^+ implantation, and the energy required was in correspondence with the TRIM [34] simulated implant projection range (R_P) to provide a similar depth of damage within the sample. Figure 4.1 compares the heating rate of both these samples without a susceptor, and confirms our theory that with the same damage and negating the impact of the susceptor, the as-implanted Si^+ heats faster than as-implanted As^+. The results presented in the figure also support our argument that materials with higher Z require assisted heating. For the same samples, when a susceptor was included in the anneal setup , the heating rates overlapped, suggesting that the effect of higher Z and differences in the factor mC_P have been overridden by the heat provided by the susceptor, as seen in Fig.4.2. The dielectric properties of the susceptor are responsible for this enhanced supply of heat to the mounted samples.

4.2. Structural Characterization

The as-implanted As^+ and the microwave annealed samples were characterized using several methods to test for dopant activation and film recrystallization. A Raman line scan was performed to determine the structure of the As^+ implanted Si pre and post microwave annealing. An argon laser with an excitation wavelength of 532 nm is focused onto the samples mounted underneath the optical microscope, through an

Olympus 100×0.8 NA objective. The spectra from the sample are reflected into a Sopra 2000 2m double spectrometer by a 50% beam-splitter. A 532 nm notch filter blocks any scattered light from the laser. The spectrum is dispersed and collected into a Princeton CCD Camera with an energy dispersion of 60pixels/cm. The Raman spectra collected from the CCD is calibrated as a function of intensity that depends on the time of exposure, against the relative wavenumber [21].

Ion channeling experiments were carried on for as-implanted Si samples with and without susceptor annealed for different times to verify once again if anneal without susceptor is capable of damage repair, and to compare the lattice damage repair by anneal with susceptor.

To observe the microstructure of the sample before and after annealing, cross-section transmission electron microscopy (XTEM) was performed using a Philips CM200 FEG TEM operated at a voltage of 200 kV. Enhancement of defect contrast was provided by 220 bright-field and dark-field imaging. TEM samples were prepared using a FEI835 focused-ion beam tool with a gallium ion-source.

4.3. Results

Raman spectra were obtained from as-implanted and annealed samples of $1\times10^{15}cm^{-2}$ dose As^{+} implanted with energy of 30 keV. In Fig.4.3 the 480 cm^{-1} broad peak is attributed to an amorphous Si layer in the unannealed samples. The Raman spectra of the annealed samples however, do not possess this peak, but instead possess a 520 cm^{-1} single crystal Si peak [16], indicating that crystallization of the as-implanted layer is not only initiated, but has been completed within 40 sec of the anneal. The smaller full width half maximum (FWHM) value implies well recrystallized Si which is the preferable outcome.

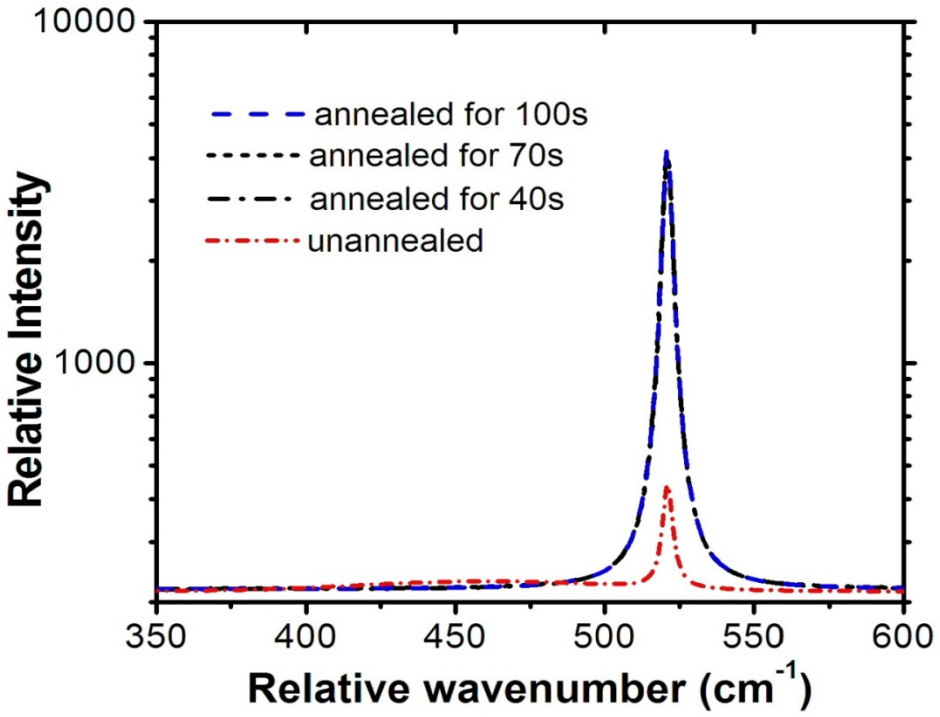

Fig. 4.3 Raman Spectra of 30 keV 1×10^{15} cm^{-2} As implanted Si after different anneal times.

Ion channeling of 75 keV 2×10^{15} cm^{-2} as-implanted Si was performed for samples annealed with susceptor for 2 minutes, and without susceptor for 6 minutes. The results as in Fig.4.4 once again prove that the susceptor brings about heating sufficient to recrystallize and repair the damage in the as-implanted Si, which cannot be achieved even after prolonged heating using the standalone microwave effect.

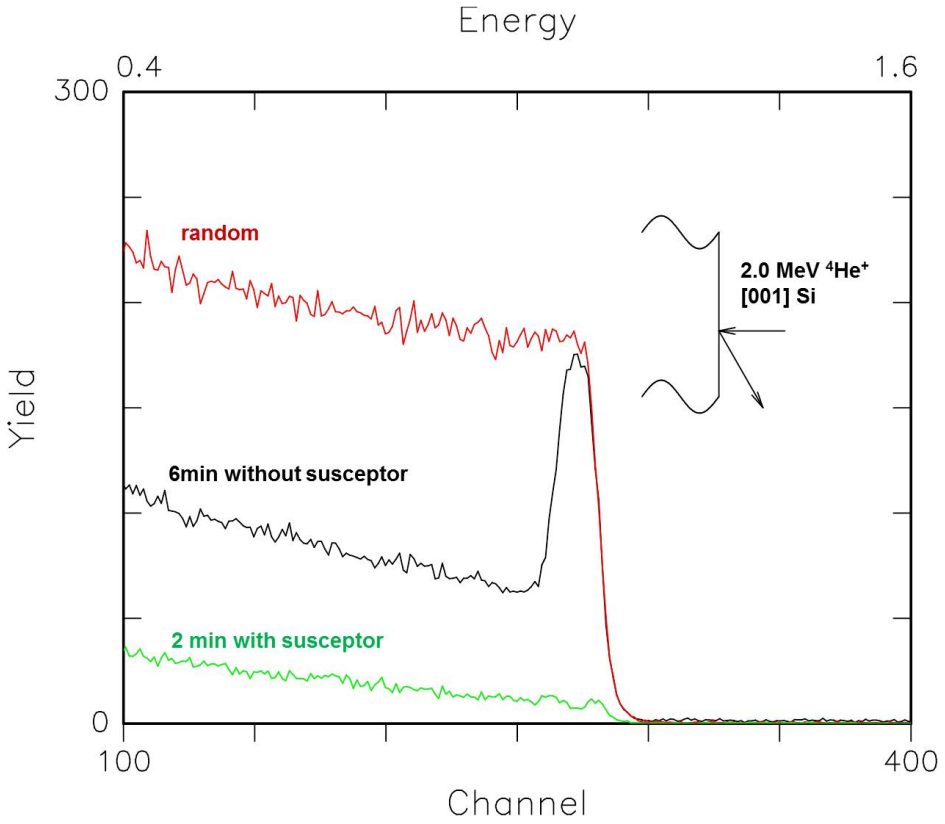

Fig. 4.4 Ion Channeling results of 75 keV 2×10^{15} cm^{-2} as-implanted Si after microwave annealing with and without susceptor. *random* profile suggests ion channeling results of an as-implanted sample in a random orientation. *6 min without susceptor* profile indicates channeling results of a 6 min annealed sample without susceptor, and *2 min with susceptor* suggests channeling results of the sample annealed for 2 minutes with susceptor.

The extent of recrystallization of the As^+ doped Si surface can be viewed from XTEM images as shown in Fig. 4.5. The amorphous layer in the as-implanted sample is distinguished from the underlying crystalline layer, as a lightly shaded region. For the microwave annealed samples of 40 sec, an amorphous layer is no more visible, and this observation supports our Raman data that the amorphous layer has been completely recrystallized. A 70 sec annealing does not provide any better results, since complete recrystallization has already been achieved. A band of defects is however observed at the depth where the amorphous-crystalline silicon layer lies in the as-implanted samples. This may be due to the migration of the vacancies to the interface [20] while the surface is being recrystallized by regrowth [15] in epitaxial fashion over the crystalline Si layer underneath. Note that a 70 sec anneal does not provide any better results, since complete recrystallization has already been achieved.

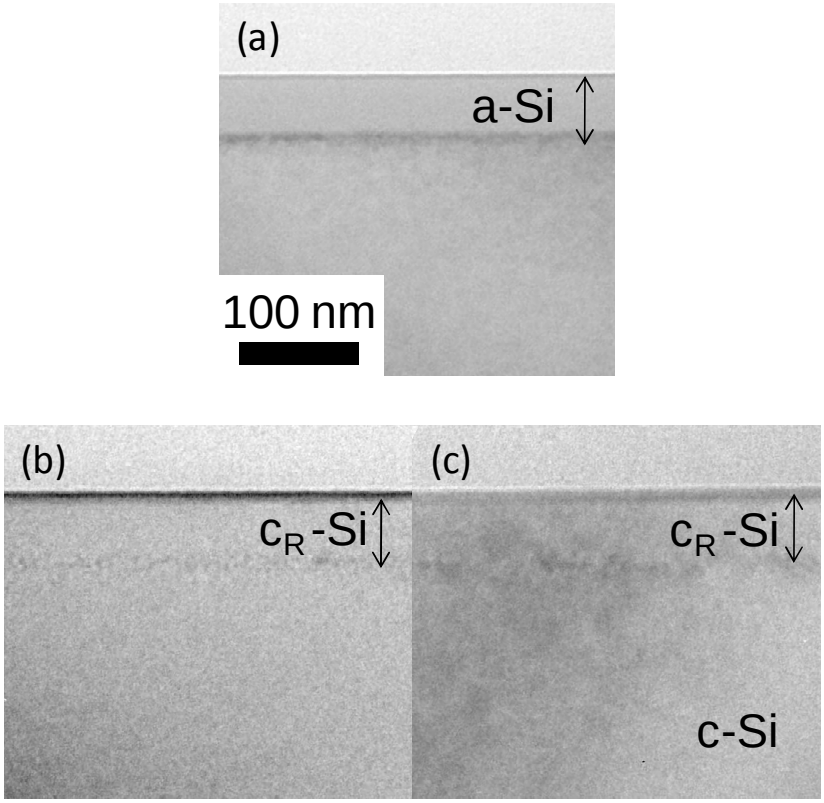

Fig. 4.5 XTEM images of Si implanted with 30 keV $1x10^{15}$ As^+ cm^{-2} (a) as implanted, (b) after 40 seconds microwave anneal and (c) after 70 seconds microwave anneal.
a-Si: amorphous Si; c-Si: crystalline Si substrate; c_R-Si: recrystallized Si region.

4.4. Discussion

Typically, a surface layer goes through incubation, before it can recrystallize due to regrowth from an underlying crystalline layer [35]. Microwaves are capable of reducing the incubation time required, hence achieving SPE in much lesser time. The advantage that microwave annealing possesses over conventional annealing is that the low temperature, which is achievable in a few seconds time (40 s in our current study), suffices for nucleation. Previous research to explore the application of microwaves shows that the interaction of the radiation with the atoms enhances diffusion properties [36] of the material. The increased diffusivity of the Silicon atoms not only provides recrystallization, but does this in a single phase, producing a single crystal from the amorphized layer [37] that has been affirmed by our Raman spectra results where the only peak observed other than a broad peak at 480cm^{-1}, is at 520cm^{-1} which is that of a single crystalline layer. The temperature of about 620 ^{o}C appears to be the key factor responsible for damage repair, but it is not enough to remove the defect bands after SPE.

From our XTEM images, a longer period of microwave annealing does not suffice to remove the defect band, which could be the only drawback amongst all of our recordings. To repair the defect network, an anneal temperature of 950 ^{o}C is required [20]. The defect band observed

is as a result of coagulation of deep level interstitials that remain from the vacancy-interstitial annihilation [20, 38]. Arsenic has a tendency to form microclusters, causing interstitials to be freed, that then form dislocations at the depth of the arsenic implant damage.

The specific heat capacity of arsenic is lower than that of silicon, making it difficult to attain higher temperatures at even the surface level of the film to facilitate a higher nucleation rate. In previous research regarding microwave annealing of boron implanted Si wafers, nucleation was achieved without a susceptor, although the boron atoms had a high C_P of 1107 J/Kg-K, due to a low atomic mass of the atom and hence a much lower mC_P factor than Si, the power absorbed from the microwave radiation was sufficient to provide increased local temperatures, and hence greater rate of solid phase epitaxy equal to $2R_P$ [20]. However, the rate of solid phase epitaxial regrowth due to conventional heating methods [39] is given by

$$v \approx \frac{\Delta g_{ca.} \delta \exp(-E_a/kT)}{h} \qquad (1)$$

where Δg_{ca} , the free energy difference between the crystalline and amorphous phases is less than kT, δ is the distance across the interface between the two phases, and E_a is the activation energy responsible for

SPE. But for arsenic implanted Si samples, high dielectric material needs to be included in the heating setup, which allows surface heating and not volumetric heating when absorbing microwave radiation. Surface heating causes a low D_P for the susceptor, which is a SiC cylinder that was filed at the mounting surface to ensure the sample placed over it had maximum surface area contact. The sample was then placed face up over the flat surface of the susceptor. This promotes the nucleation of the crystalline phase upwards at the interface through the amorphous layer of the film, because of the high upward flux of heat [40] from the susceptor. The upward heat flux of this high temperature, then increases the local temperature of arsenic atoms at the interface of crystalline and amorphous silicon, and provides a higher nucleation rate to the sites, just as the metal impurities do in the MIC annealing method. Equation 1 gives a lesser SPE rate compared to nucleating rate of twice the projected implant range *i.e.,* $2R_P$ [41, 42] achieved by microwave annealing, making the latter preferable.

4.5. Conclusion

The susceptor is not only successful in providing the advantage of higher temperature and higher SPE growth velocity, but it does so without the addition of metal impurities into the samples. The rate of regrowth is also much higher compared to regular regrowth method. The studies suggest that the susceptor assisted microwave annealing can be a suitable alternative post implantation processing technique with improvements on magnetron used in the microwave cavity and further care in choosing the ambient.

Chapter 5

SUMMARY

5.1. Introduction

This chapter discussed the industry needs and concerns regarding processes involved in treating ion implanted materials. The post implantation processing techniques commonly used, such as laser anneal, metal induced crystallization, and rapid thermal anneal have were explained in brief. The disadvantages caused due to each of these methods were the motivation behind the study of microwave anneal as an alternative process technique. Knowledge of microwave technology was necessary to perform the study, which has been explained in great detail in this chapter The microwave anneal has been found to be due to loss mechanisms, and dielectric properties of the material. This knowledge gives us an understanding of how anneal process would effect different materials differently, and what considerations can be made while annealing materials with different properties. For example, previous research of boron implanted Si, and our study of arsenic implanted Si shows that, though the underlying post implantation process is microwave anneal, were treated differently due to the properties of the samples. Hence, in our study, a susceptor providing surface heating was necessitated to allow the sample to absorb the microwave radiation and undergo volumetric heating.

5.2 Materials Characterization

The As implanted Si, and as-implanted Si samples were annealed for various time durations in the microwave cavity applicator by incorporating the susceptor into the setup. A few runs of the experiment were repeated by eliminating the use of the susceptor. To observe the material properties pre and post anneal, several characterization techniques were used. The samples were characterized to observe differences in structure, topology, and electrical properties before and after anneal. Electrical characterization using four point probe measurements and Hall measurements provided sheet resistance, resistivity, mobility, and sheet concentration information. Ion channeling was performed on the samples to ascertain the extent of damage repair possible by microwave anneal mechanism. Cross-section transmission electron microscopy (XTEM) patterns provided information on structural changes caused by annealing. Raman spectroscopy also provided extent of damage repair or recrystallization of the samples. Secondary ion mass spectrometry (SIMS) was performed to verify if the anneal process caused any undesired dopant diffusion into the substrate. Each of these characterization techniques were explained in detail in chapter 2.

5.3 Dopant Activation and Dopant Diffusion of As implanted Si

The As implanted Si samples of different dosage and implantation energy were annealed for different times with susceptor, and electrical characterization techniques such as 4-point probe and Hall measurements were used to derive data to verify dopant activation and dopant diffusion. Microwave anneal process was successful in electrically activating the dopants, suggested by low sheet resistances, and high sheet concentrations. Ion channeling data supports dopant activation by the relocation of dopant atoms into substitutional sites instead of off-lattice sites. SIMS was performed to analyze any possible dopant diffusion, comparing the results against a 30 second annealed sample at 900 ℃. The results indicated minimal dopant diffusion using microwave anneal. The microwave heating mechanism was discussed in detail supporting the use of a susceptor to obtain quick recrystallization, and dopant activation, and minimum dopant diffusion in As implanted Si.

5.4 Recrystallization of As implanted Si and as-implanted Si

Arsenic implanted, and silicon implanted Si samples, of the same extent of damage were considered. The influence of material properites on anneal mechanism was proved by annealing the 2 types of samples without susceptor. The samples were annealed both with, and without susceptor for different durations. Raman spectroscopy was performed, which provided data supporting quick recrystallization providing a good quality single crystal Si by recrystallization. Ion channeling was also performed on as-implanted Si annealed with and without susceptor, showing no damage repair of the lattice when a susceptor was not used. XTEM images confirm the recrystallization of the entire amorphized layer of the As implanted Si samples. The rate of recrystallization obtained by microwave anneal were compared to the rate of recrystallization due to solid phase epitaxy, and the microwave anneal was found to produce a higher rate of regrowth.

5.5 Conclusion

This thesis work supports the microwave anneal technique as an alternate post implantation process technique. The innovative use of a susceptor to provide additional heating to a high *Z* material like As, not only brought about faster recrystallization and dopant activation, but also provided desirable results interms of dopant diffusion by indicating minimum diffusion of As into the Si. The susceptor's surface heating also enabled the formation of a good quality single crystal doped Si, instead of formation of poly-Si which is possible due to insufficient heating. The successful recrystallization of the high energy implanted samples suggests that irrespective of the damage, the susceptor assisted anneal can provide heating sufficient to overcome the high activation energy required to form single crystal Si, and facilitate quick recrystallization of a thick damaged layer.

5.6 Future Work

In order to incorporate the microwave anneal technology into the current industry requirements operating at a 17 nm node, further research can be performed on low energy implanted samples. Also, focus can be laid on achieving zero dopant diffusion. Efforts should be put into achieving a defect free interface layer. The effect of increased magnetron power can be studied to provide the defect free interface upon recrystallization.

REFERENCES

[1] Y. Lee, F. Hsueh, S.Huang, J. Kowalski, A. Cheng, A. Koo, G.L.Luo, and C.Y.Wu, “A low-temperature microwave anneal process for boron-doped ultrathin Geepilayer on Si substrate”, IEEE Electron Dev. Lett., vol. 30, no. 2, pp. 123-125, 2009.

[2] K. M. Klein, C. Park, and A. F. Tasch, Appl. Phys. Lett., **57**, 25 (1990)

[3] K. M. Klein, C. Park, and A. F. Tasch, Nuc. Instr. And Meth. in Phys. Res., **B59/60**, 60 (1991)

[4] C. Tian, S.Gara, G. Hobler, and G. Stingeder, Microchimica Acta, **107**, 161 (1992)

[5] G. Pepponi, D. Giubertoni, S. Gennaro, M. Bersani, M. Anderle, R. Grisenti, M. Werner, and J. A. van den Berg, in *Ion Implantation Technology*, Marseille, France, edited by K. J. Kirkby, R. Gwilliam, A. Smith, and D. Chivers (AIP, New York, 2006),117 (2006)

[6] J.Ahn, J. Lee, Y.Kim, and B.Ahn, Current Applied Physics, 2, 135, (2002).

[7] Y. Lee, F. Hsueh, S.Huang, J. Kowalski, A. Cheng, A. Koo, G. Luo, and C. Wu, IEEE Electron Device Letters, **30 (2)**, 123 (2009).

[8] J. W. Mayer and S. S. Lau, Electronic Materials Science: For Integrated Circuits in Si and GaAs, Macmillan, New York, (1990)

[9] T.Matsuyama, N.Terada, T. Baba, T. Sawada, S. Tsuge, K. Wakisaka, and S.Tsuda, J Non-Cryst Solids, **940**, 198 (1996).

[10] R.B. Bergmann, G. Oswald, M. Albrecht, Gross V. SolEnergy Mater Sol Cells, **46**, 147 (1997).

[11] K. Ishikawa, M. Ozawa, C. Oh , and M. Matsumura, Jpn J. Appl. Phys. **37**, 731 (1998).

[12] R. Kakkad, J. Smith, W.S. Lau, S.J. Fonash, and R. Kerns, J. Appl. Phys. 65, 206 (1989).

[13] G. Huang, Z. Xi, and D. Yang, Vacuum **80,** 415 (2006).

[14] L. Hultman, A. Robertsson , H.T.G Hentzell, I. Engstrom, and PA. Psaras, J Appl Phys, **62**, 3647 (1987).

[15] Y.Woo, K.Kang, M.Jo, J.Jeon, and Miyoung Kim, Appl Phys Lett, **91**, 223107 (2007).

[16] S. C. Fong, C. Y. Wang, T. H. Chang, and T. S. Chin, Appl Phys Lett, **94**, 102104 (2009)

[17] R. E. Newnham, S. J. Jang, M. Xu, and F. Jones. Fundamental Interaction Mechanisms Between Microwaves and Matter. Ceramic Transactions, Microwaves: Theory and Application in Materials Processing, **21** (1991)

[18] C.Kittel, Solid State Physics, 2nd ed., New York: John Wiley and Sons (1959)

[19] P.Debye, Polar Molecules, Chemical Catalog Co., New York (1929)

[20] D. C. Thompson, J. Decker, T. L. Alford, J. W. Mayer, and N. D. Theodore, Mater. Res. Soc. Symp. Proc, **989**, A06-18 (2007)

[21] C.D.Poweleit, A.Gunther, S.Goodnick, and J. Mene´ndez, Appl Phys Lett, **73**, 16 (1998)

[22] W. K. Chu, J. W. Mayer, and M. A. Nicolet, Backscattering Spectroscopy (Academic press, San Diego, CA), 4, (1978).

[23] L. A. Giannuzzi, F. A. Stevie, *Introduction to Focused Ion Beams*, (2005).

[24] R. Rao and G.C. Sun, Journal of Crystal Growth, **273**, 68 (2004)

[25] T. L. Alford, D. C. Thompson, J. W. Mayer, and N. D. Theodore, J. Appl. Phys. **106**, 114902 (2009)

[26] T. L. Alford, L. C. Feldman, and J. W. Mayer, Fundamentals of Nanoscale Film Analysis (Springer, New York, 2008)

[27] A. C. Metaxas and R. J. Meredith, Industrial Microwave Heating, IEEE Power Engineering Series **4** (Peter Peregrinus, London, 1983)

[28] W.H. Sutton, Am. Ceram. Soc. Bull. **68 (2)**, 376 (1989)

[29] D. E. Clark, D. C. Folz, J. K. West, Mat. Science and Engineering **A287**, 153 (2000)

[30] D. R. Gaskell, *Introduction to the Thermodynamics of Materials,* Taylor & Francis, Levittown, PA, (1995)

[31] M. M. Bulbul, Microelectronic Engineering, **84**, 124 (2007)

[32] A. I. Shkrebtii, Z. A. Ibrahim, T. Teatro, W. Richter, M.J.G. Lee, and L. Henderson, Phys. Status Solidi **B 247(8)**, 1881 (2010)

[33] W.Bohmayr, A.Burenkov, J.Lorenz, H.Ryssel, S.Selberherr, IEEE Transactions on Computer-Aided Design of Integrated Circuits and Systems, **17 (12)**, 1236 (1998)

[34] G.M.Crean, P.D.Cole, C.Jeynes, Solid State Electronics, **33 (6)**, 655 (1990)

[35] E. Kinsbron, M.Sternheim, and R.Knoell, Appl. Phys. Lett., **42**, 835 (1983)

[36] M. A. Janney, H. D. Kimrey, M. A. Schmiat, and J. O. Kiggan, J. Am. Ceram. Soc. **74**, 1675 (1991)

[37] J. N. Lee, Y.W. Choi, B. J. Lee, and B.T. Ahn, J. Appl. Phys. **82,** 6 (1997)

[38] S. N. Hsu and L. J. Chen, Appl. Phys. Lett., **55 (22)**, 2305 (1989)

[39] J. W. Christian, *The Theory of Transformations in Metals and Alloys, Part 1*, 3rd ed. Elsevier Science, Oxford, Version 1, **Chap. 11**, 482 (2002)

[40] S.M. Zanetti, J.S. Vasconcelos, N.S.L.S. Vasconcelos, E.R. Leite, E. Longo, and J.A. Varela, Thin Solid Films, **466**, 62 (2004)

[41] J. W. Mayer, S. S. Lau, *Electronic Materials Science: For Integrated Circuits in Si and GaAs*, Macmillan Publishing Company, New York, NY (1990)

[42] J. D. Plummer, M. D. Deal, P. B. Griffin, *Silicon VLSI Technology: Fundamentals, Practice and Modeling*, Prentice Hall, Upper Saddle River, NJ (2000).